arXiv:1006.5184v1 [astro-ph.GA] 27 Jun 2010

Switched magnetospheric regulation of pulsar spin-down

Andrew Lyne,[1*] George Hobbs,[2] Michael Kramer,[1,3] Ingrid Stairs,[4] Ben Stappers[1]

[1] Jodrell Bank Centre for Astrophysics, School of Physics and Astronomy, University of Manchester, Manchester, M13 9PL, UK

[2] Australia Telescope National Facility, CSIRO, PO Box 76, Epping NSW 1710, Australia

[3] MPI für Radioastronomie, Auf dem Hügel 69, 53121 Bonn, Germany

[4] Dept. of Physics and Astronomy, University of British Columbia, 6224 Agricultural Road, Vancouver, BC V6T 1Z1, Canada

*To whom correspondence should be addressed; E-mail: andrew.lyne@manchester.ac.uk.

Pulsars are famed for their rotational clock-like stability and their highly-repeatable pulse shapes. However, it has long been known that there are unexplained deviations (often termed "timing noise") from the rate at which we predict these clocks should run. We show that timing behaviour often results from typically two different spin-down rates. Pulsars switch abruptly between these states, often quasi-periodically, leading to the observed spin-down patterns. We show that for six pulsars the timing noise is correlated with changes in the pulse shape. Many pulsar phenomena including mode-changing, nulling, intermittency, pulse shape variability and timing noise are therefore linked and caused by changes in the pulsar's magnetosphere. We consider the possibility that high-precision monitoring of pulse profiles could lead to the formation of highly-stable pulsar clocks.

Introduction

Neutron stars form in the supernova collapse of the cores of exhausted massive stars and are comprised of some of the densest and most extreme matter in the observable Universe. Pulsars are rapidly-rotating, highly-magnetized neutron stars. As they rotate, intense beams of electromagnetic radiation may sweep across the Earth, resulting in pulses which are often observed with radio telescopes, enabling their rotation to be studied with high precision.

Pulsars are amongst the most stable rotators known in the Universe. Over long time spans the fastest spinning pulsars known as "millisecond pulsars" even rival the stability of atomic clocks (*1*). Although they slow down gradually because of the conversion of rotational energy into highly energetic particles and electromagnetic waves, a simple spin-down model using only the pulsar's rotational frequency ν and its first time derivative $\dot{\nu}$ is often sufficient to reveal timing properties that, for instance, allow high-precision tests of the theory of general relativity (*2*) and may also allow direct detection of gravitational waves (*3–5*). However, not all pulsars seem to be perfectly stable clocks.

The pulsar timing technique (*6, 7*) is used to compare pulse arrival times at an observatory with times predicted from a spin-down model. Many pulsars show a phenomenon known as "timing noise" where seemingly quasi-random walks in the rotational parameters are observed. The largest study of such kind (*2*) recently presented the rotation properties of 366 pulsars, measured mainly using the Lovell Telescope at Jodrell Bank. This long-term monitoring of pulsars over 40 years made it possible to study phenomena in many pulsars over decadal timescales. It was shown that the majority of the pulsars were found to have significant irregularities in their rotation rate. The differences between the observed and predicted times, known as the pulsar "timing residuals", can be less than a few milliseconds over more than 30 yr, but in other cases timing residuals can be as large as many seconds. In contrast to the standard models held for

the past $\sim$40 yr, it was found that these timing irregularities are often quasi-periodic with long ($\sim$1-10 year) time scales. Here we present a description of these irregularities and how they are related to changes in pulse shape, linking many peculiar and unexplained time-dependent phenomena observed in pulsars.

Pulsar Time Scales

Many of the properties of pulsars are not perfectly stable and they vary over a wide range of timescales. Rotational periods range from milliseconds to seconds. The structure and brightness of individual pulses are observed to vary significantly, but the average of many hundreds of individual pulses ($\sim$minutes) is usually stable, leading to a characteristic profile that is often unique to a pulsar. On time scales of seconds to hours, some pulsars are observed to exhibit either "nulling" events, during which the pulse emission switches "off", or "mode changing" events where the observed pulse profile changes abruptly between two (sometimes three) well-defined shapes. On longer time scales, PSR B1931+24 has recently been described as an "intermittent pulsar" which relates to the fact that it undergoes extreme nulling events (*9*), displaying quasi-periodic behaviour in which the pulsar acts as a normal pulsar for typically five to ten days, before switching "off", being undetectable for $\sim$25 days and then abruptly switching "on" again. On even longer time scales, stable harmonically-related periodicities of $\sim$250, 500 and 1000 d, have been reported in the rotation rate and pulse shape of PSR B1828$-$11. The periodicities have generally been interpreted as being caused by PSR B1828$-$11 freely-precessing (*1*), even though it had been argued that this was not possible in the presence of the superfluid component believed to exist inside neutron stars (*11*).

Discrete pulsar spin-down states

The patterns observed in the timing residuals of a sample of 10 pulsars (Fig. 1) are typical of the sample presented in (*2*) and highlight the main results of that paper that 1) the residuals are dominated by quasi-periodic structures and 2) the residuals are generally asymmetric, in that the radii of curvature of local maxima are often consistently different to those of local minima. Clear examples are seen in PSRs B0950+08, B1642−03, B1818−04, B1826−17 and B1828−11. In several cases, notably PSRs B0919+06 and B1929+20, relatively rapid oscillations lie on lower-frequency structures.

Structures in the timing residuals have been widely discussed in the literature. Sudden increases in the pulsar's rotation rate are known as "glitches" and are explained by the sudden unpinning of superfluid vortices in the interior of the neutron star (*12*). An apparently related phenomenon known as "slow glitches" has been described (*13, 14*), characterised by a slow permanent increase in rotation rate but no substantial change in the slow-down rate and also identified with the interior of the neutron star. The low-frequency structures seen over short data spans were thought to represent either random walks in the pulse frequency and/or its derivatives (*15, 16*) arising from instabilities within the neutron star superfluid interior, multiple micro-glitches (*17*), free precession of the neutron star (*1*), asteroid belts (*18*), magnetospheric effects (*19*), interstellar or interplanetary medium effects (*20*) or accretion of material onto the pulsar's surface (*21*). Timing residuals for the youngest pulsars in (*2*) are dominated by the recovery from glitch events, sometimes having occurred prior to the start of observing. In general, for the remaining pulsars it was shown that, with long data spans, the low-frequency structures are no longer dominant, but are now understood as restricted pieces of much longer-term oscillatory structures, often with asymmetric maxima and minima. Any model explaining timing noise therefore needs to explain these commonly-occurring features.

The analysis of PSR B1931+24 (*9*) showed that the pulsar spin-down rate switched by $\sim$50% between the "on" and "off" states, with the pulsar spinning down faster when the radio signal was detectable. The quasi-periodic nature of the time between state changes and the difference in time spent in each state leads naturally to oscillatory, asymmetric timing residuals (Fig. 6). The existence of two discrete spin-down rates in PSR B1931+24 and the similarities between such timing residuals and those shown in Fig. 1 suggests that a similar model could be also applied to the timing noise seen in all pulsars.

The variation in the spin-down rate $\dot{\nu}(t)$ for 17 pulsars demonstrates that the observed structures in the timing residuals arise from a pulsar's $\dot{\nu}$ moving between a small number of values and frequently in an oscillatory manner (Fig. 2). In some cases more complex structure is seen. For instance, in PSR B1642$-$03 we observe peaks in $\dot{\nu}$ followed by a sudden change to a more negative $\dot{\nu}$ value before a slow gradual rise. In PSR B1828$-$11, in addition to the oscillatory structure, we also observe a long-term gradual linear change in $\dot{\nu}$ across the data span. We concentrate on the dominant features of this figure: the value of $\dot{\nu}$ changes between a few (typically two) well-defined values, often in a quasi-periodic manner.

In order to quantify the behaviour, we measured the peak-to-peak values of $\dot{\nu}$ for each pulsar (Table 1). Additionally, for each of the time sequences in Fig. 2, we have performed Lomb-Scargle (*22*) and wavelet (*23*) spectral analyses. As expected, some of the resultant spectra (Figs. 7 and 8) show narrow, highly-periodic features, while others show broader, less well-defined peaks.

Pulse shape variations

Following the implications of the study of PSR B1931+24 that changes within the magnetosphere are responsible for variations in both the spin-down rate and the emission process (*9*), we have sought changes in the pulse shapes of those pulsars which have shown the greatest frac-

tional changes in spin-down rate in the timing noise study. Six pulsars show changes in pulse shape which are clearly visible (Fig. 3). From inspection of the profiles in Fig. 3, for each pulsar we selected the simplest "shape parameter" which would discriminate between the two extreme pulse-shape states, such as W_{10}, W_{50} or W_{75}, the full widths at 10%, 50% or 75%, or $W_{\rm eq}$, the equivalent width (see the Supporting Online Material for details on how these were determined and their implications for the timing residuals). For six pulsars, the observed changes in $\dot{\nu}$ are indeed directly related to changes in pulse shape (Fig. 4). In most cases, the two quantities clearly track one another and there is strong evidence for either correlation or anti-correlation in all six cases (Fig. 9). It is not clear whether the imperfect correlations are intrinsic or arise from the sparse sampling of the time series or measurement errors.

Some of the pulse profiles suggest that increased $|\dot{\nu}|$ is associated with increased amplitude of the central (often described as "core") emission relative to the surrounding (or "conal") emission (Fig. 3). PSR B1822−09 exhibits a main pulse, a precursor and an interpulse (*24, 25*). For the high $|\dot{\nu}|$ state the precursor is weak and the interpulse is strong, the reverse occurring for the smaller $|\dot{\nu}|$ state. Clearly, some changes in $\dot{\nu}$ are associated with large profile changes (e.g. PSRs J2043+2740 and B1822−09) while smaller profile changes are also observable if sufficiently high-quality data are available (e.g. PSR B1540−06).

While the main impression given by the traces in Fig. 4 is that they are bounded by two extreme levels, there are substantial, and often repeated, subtle changes which are synchronised in both shape parameter and $\dot{\nu}$. The shape parameters for the observations of PSRs B1822−09, B1828−11 and B2035+36 imply that they spend most of the time in just one extreme state or the other. This is essentially the phenomenon of mode-changing, which has been known since shortly after the discovery of pulsars (*24, 26–28*). In those papers, pulsars are reported to show stable profiles, but suddenly switch to another stable mode for times ranging from minutes to hours. However, the time-averaged values of the shape parameters depend upon the

mix of the two states over the averaging period and that varies with time, causing the slower changes in the shape-parameter curves and the spin-down rate curves. $\sim$2500 d of detail in the shape parameters and spin-down rates of PSRs B1822$-$09 and B1828$-$11 (Fig. 5) illustrate how a slowly-changing mix of the two states is reflected in the form of the smoothed shape curves. In PSR B1822$-$09, the events centered on MJDs 51100 and 52050 are the sites of slow glitches (*13, 14*) which we confirm are not a unique phenomenon (*2*), but arise from short periods of time spent predominantly in a small-$|\dot{\nu}|$, large-precursor mode.

Discussion

The large number of pulsars observed over many years in the Jodrell Bank data archive has allowed the identification of a substantial number of pulsars that have large $\dot{\nu}$ changes, some of which also have detectable, correlated pulse-shape changes. This correlation indicates that the causes of these phenomena are linked and are magnetospheric in origin. The physical mechanism for this link is likely to be that suggested to explain the relationship between spin-down rate and radio emission in B1931+24, namely a change in magnetospheric particle current flow (*9*). An enhanced flow of charged particles causes an increase in the braking torque on the neutron star and also in the emission radio waves.

The link between the spin-down rate and radio-emission properties has not been established previously, mainly because the timescales of the long-established phenomena of mode-changing and pulse-nulling were much shorter than the time required to measure any change in $\dot{\nu}$. The extended high-quality monitoring of many pulsars has now revealed long-term manifestations of these phenomena and allowed their unambiguous association with the spin-down rates of pulsars, seen as timing noise. Pulsars can spend long periods of time in one magnetospheric state or another or in some cases switch rapidly back and forth between states, the fractions of time spent in the two states often varying with time. It has long been suspected that mode-

changing and nulling are closely related [e.g. (*29*, *30*)]. The intermittent pulsar B1931+24 has the largest fractional change in $\dot{\nu}$ in Table 1 and, as it completely disappears, also has the largest apparent change in pulse shape. Mode-changing and nulling therefore probably differ only in the magnitude of the changes in the magnetospheric current flows. There is a close linear relationship between $\Delta\dot{\nu}$ and the spin-down rate $|\dot{\nu}|$ (Fig. 10), indicating that the value of $\dot{\nu}$ switches by about 1% of the mean value, independent of its magnitude.

We must also emphasise that: (1) the fast change between the states indicates that the magnetospheric state changes on a fast time scale, but can then be stable for many months or years before undergoing another fast change, (2) whatever the cause of the state-switching, for most pulsars, it is not driven by a highly periodic (high-Q) oscillation and (3) increased $|\dot{\nu}|$ is associated with increased amplitude of the core emission relative to conal emission. The fast state-changes seem to rule out free precession as the origin of the oscillatory behaviour. PSR B1828$-$11 was considered unique in that it was the only pulsar that showed clear evidence for free precession (*1*). Our model indicates that this pulsar is not unique and exhibits the same state-changing phenomenon shown here for other pulsars.

If we could monitor a pulsar continuously, then its magnetospheric state at any given time could be determined from the pulse shape. The state gives a measure of the spin-down rate, allowing the timing noise to be removed (an example is given in Fig. 6). The most stable millisecond pulsars are being regularly observed from many observatories world-wide in the hope of making the first direct detection of gravitational waves . The first-discovered millisecond pulsar, PSR B1937+21, can be timed with high precision (of ~ 100 ns) over short data spans, but low-frequency timing irregularities dominate the timing residuals over data spanning more than ~ 3 yr (*32*) making this pulsar potentially unusable for gravitational wave detection experiments. However, if magnetospheric state switching is responsible and can be applied to millisecond pulsars, then the timing irregularities can be modelled and removed, raising the

possibility of producing an essentially stable clock.

References and Notes

1. G. Petit, P. Tavella, *A&A* **308**, 290 (1996).
2. M. Kramer, *et al.*, *Science* **314**, 97 (2006).
3. M. V. Sazhin, *Sov. Astron.* **22**, 36 (1978).
4. S. Detweiler, *ApJ* **234**, 1100 (1979).
5. F. A. Jenet, G. B. Hobbs, K. J. Lee, R. N. Manchester, *ApJ* **625**, L123 (2005).
6. D. R. Lorimer, M. Kramer, *Handbook of Pulsar Astronomy* (Cambridge University Press, 2005).
7. R. T. Edwards, G. B. Hobbs, R. N. Manchester, *MNRAS* **372**, 1549 (2006).
8. G. Hobbs, A. G. Lyne, M. Kramer, *MNRAS* **402**, 1027 (2010).
9. M. Kramer, A. G. Lyne, J. T. O'Brien, C. A. Jordan, D. R. Lorimer, *Science* **312**, 549 (2006).
10. I. H. Stairs, A. G. Lyne, S. Shemar, *Nature* **406**, 484 (2000).
11. J. Shaham, *ApJ* **214**, 251 (1977).
12. P. W. Anderson, N. Itoh, *Nature* **256**, 25 (1975).
13. W. Z. Zou, *et al.*, *MNRAS* **354**, 811 (2004).
14. T. V. Shabanova, *Astrophys. Space Sci.* **308**, 591 (2007).

15. P. E. Boynton, *et al.*, *ApJ* **175**, 217 (1972).

16. J. M. Cordes, G. S. Downs, *ApJS* **59**, 343 (1985).

17. G. H. Janssen, B. W. Stappers, *A&A* **457**, 611 (2006).

18. J. M. Cordes, R. M. Shannon, *ApJ* **682**, 1152 (2008).

19. K. S. Cheng, *ApJ* **321**, 799 (1987).

20. K. Scherer, H. Fichtner, J. D. Anderson, E. L. Lau, *Science* **278**, 1919 (1997).

21. G. J. Qiao, Y. Q. Xue, R. X. Xu, H. G. Wang, B. W. Xiao, *A&A* **407**, L25 (2003).

22. J. D. Scargle, *ApJ* **263**, 835 (1982).

23. G. Foster, *AJ* **112**, 1709 (1996).

24. L. A. Fowler, D. Morris, G. A. E. Wright, *A&A* **93**, 54 (1981).

25. D. Morris, D. A. Graham, N. Bartel, *MNRAS* **194**, 7P (1981).

26. D. C. Backer, *Nature* **228**, 1297 (1970).

27. A. G. Lyne, *MNRAS* **153**, 27P (1971).

28. D. Morris, W. Sieber, D. C. Ferguson, N. Bartel, *A&A* **84**, 260 (1980).

29. A. G. Lyne, F. G. Smith, *Pulsar Astronomy, 3rd ed.* (Cambridge University Press, Cambridge, 2005).

30. N. Wang, R. N. Manchester, S. Johnston, *MNRAS* **377**, 1383 (2007).

31. G. Hobbs, *AIP Conf. Series*, Y.-F. Yuan, X.-D. Li, D. Lai, eds. (2008), vol. 968 of *AIP Conf. Series*, pp. 173–180.

32. V. M. Kaspi, J. H. Taylor, M. Ryba, *ApJ* **428**, 713 (1994).

33. G. B. Hobbs, R. T. Edwards, R. N. Manchester, *MNRAS* **369**, 655 (2006).

34. Pulsar research at JBCA is supported by a Rolling Grant from the UK Science and Technology Facilities Council.

GH is the recipient of an Australian Research Council QEII Fellowship (#DP0878388).

MK is supported by a salary from the Max-Planck Society.

Pulsar research at UBC is supported by an NSERC Discovery Grant.

Table 1: Measured parameters of 17 pulsars presented in Fig. 2, as well as PSR B1931+24 which is also discussed in the text. We give the pulsar names, rotational frequency ν and the first derivative $\dot{\nu}$, followed by the peak-to-peak fractional amplitude $\Delta\dot{\nu}/\dot{\nu}$ of the variation seen in Fig. 2. The pulsars are given in order of decreasing value of this quantity. We also present the fluctuation frequencies F of the peaks of the Lomb-Scargle power spectra (Fig. 7), with the widths of the peaks or group of peaks given in parenthesis in units of the last quoted digit.

Pulsar name	Jname	ν (Hz)	$\dot{\nu}$ (Hz s^{-15})	$\Delta\dot{\nu}/\dot{\nu}$ (%)	F (yr^{-1})	Comment
B1931+24[a]	J1933+2421	1.229	−12.25	44.90	13.1(7)	Intermittent pulsar
B2035+36	J2037+3621	1.616	−12.05	13.28	0.02(2)	28% change in W_{eq}
B1903+07	J1905+0709	1.543	−11.76	6.80	0.36(13)	
J2043+2740	J2043+2740	10.40	−135.36	5.91	0.11(5)	100% change in W_{50}
B1822−09	J1825−0935	1.300	−88.31	3.28	0.40(7)	100% change in A_{pc}/A_{mp}
B1642−03	J1645−0317	2.579	−11.84	2.53	0.26(7)	
B1839+09	J1841+0912	2.622	−7.50	2.00	1.00(15)	
B1540−06	J1543−0620	1.410	−1.75	1.71	0.24(2)	12% change in W_{10}
B2148+63	J2149+6329	2.631	−1.18	1.69	0.33(7)	
B1818−04	J1820−0427	1.672	−17.70	0.85	0.11(1)	
B0950+08	J0953+0755	3.952	−3.59	0.84	0.07(3)	
B1714−34	J1717−3425	1.524	−22.75	0.79	0.26(4)	
B1907+00	J1909+0007	0.983	−5.33	0.75	0.15(2)	
B1828−11	J1830−1059	2.469	−365.68	0.71	0.73(2)[b]	100% change in W_{10}
B1826−17	J1829−1751	3.256	−58.85	0.68	0.33(2)	
B0919+06	J0922+0638	2.322	−73.96	0.68	0.62(4)	
B0740−28	J0742−2822	5.996	−604.36	0.66	2.70(20)	20% change in W_{75}
B1929+20	J1932+2020	3.728	−58.64	0.31	0.59(2)	

[a]Data from reference (*9*).
[b]Note the presence of a second harmonic at F=1.47(2) yr^{-1} seen in Fig. 7 and discussed in (*1*).

Fig. 1. Pulsar timing residuals relative to a simple spin-down model of the pulse frequency and its first derivative. For PSRs B0919−06, B1540−06 and B1828−11 we have also included the frequency second derivative in the model. For each pulsar, the peak-to-peak range in residual is given, and the vertical scale has been adjusted to give the same peak-to-peak deflection in the diagram. We use data updated from those presented in (*2*) and also include data for PSR J2043+2740. The residuals were obtained using the TEMPO2 software package (*33*).

Fig. 2. Variations in the spin-down rate $\dot{\nu}$ for 17 pulsars during the past 20 years. We determined these values by selecting small sections of data of length T and fitting for values of ν and $\dot{\nu}$, repeating at intervals of $\sim$T/4 through each data set. The chosen value of T is the smallest required to provide sufficient precision in $\dot{\nu}$ and is given below each pulsar name. T is typically 100-400 d so that any short-time-scale variations will be smoothed out. For each pulsar, we adjusted the vertical scale to give the same peak-to-peak amplitude and subtracted an arbitrary vertical offset. Because $\dot{\nu}$ is negative, an increase in the rate of spin-down is represented by a downward deflection in this diagram.

Fig. 3. The integrated profiles at 1400 MHz of six pulsars which show long-term pulse-shape changes. For each pulsar, the two traces represent examples of the most extreme pulse shapes observed. The profile drawn in the thick line corresponds to the largest rate of spin-down $|\dot{\nu}|$. The profiles are scaled so that the peak flux density is approximately the same. PSR B1822−09 has an interpulse which is displayed, shifted by half the pulse period, in the second trace below the main pulse.

Fig. 4. The average value of pulse shape parameter and spin-down rate $\dot{\nu}$ measured for six pulsars. The lower trace in each panel (right-hand scale) shows the same values of $\dot{\nu}$ given in Fig. 2, while the upper trace gives a measure of the pulse shape, with the scale given to the left. W_{10}, W_{50} and W_{75} are the full widths of the pulse profile at 10%, 50% and 75% of the peak pulse amplitude respectively, W_{eq} is the pulse equivalent width, the ratio of the area under the

pulse to the peak pulse amplitude, and A_{pc}/A_{mp} is the ratio of the amplitudes of the precursor and main pulse. The time over which a shape parameter is averaged is the same as the time T given in Fig. 2 for the fitting of $\dot{\nu}$. The uncertainty on a shape parameter is derived from the standard deviation of the individual values used to determine the average.

Fig. 5. The variations in pulse shape parameters for PSR B1822−09 (a-c) and PSR B1828−11 (d-f). Traces a, c, d and f are taken from Fig. 4 and show the smoothed values of shape parameter and spin-down rate for the two pulsars, while diagrams b and e show the values of shape parameter for individual observations which are typically between 6 and 18 minutes duration. Note that for both pulsars, individual shape parameter values typically take either a high or low value.

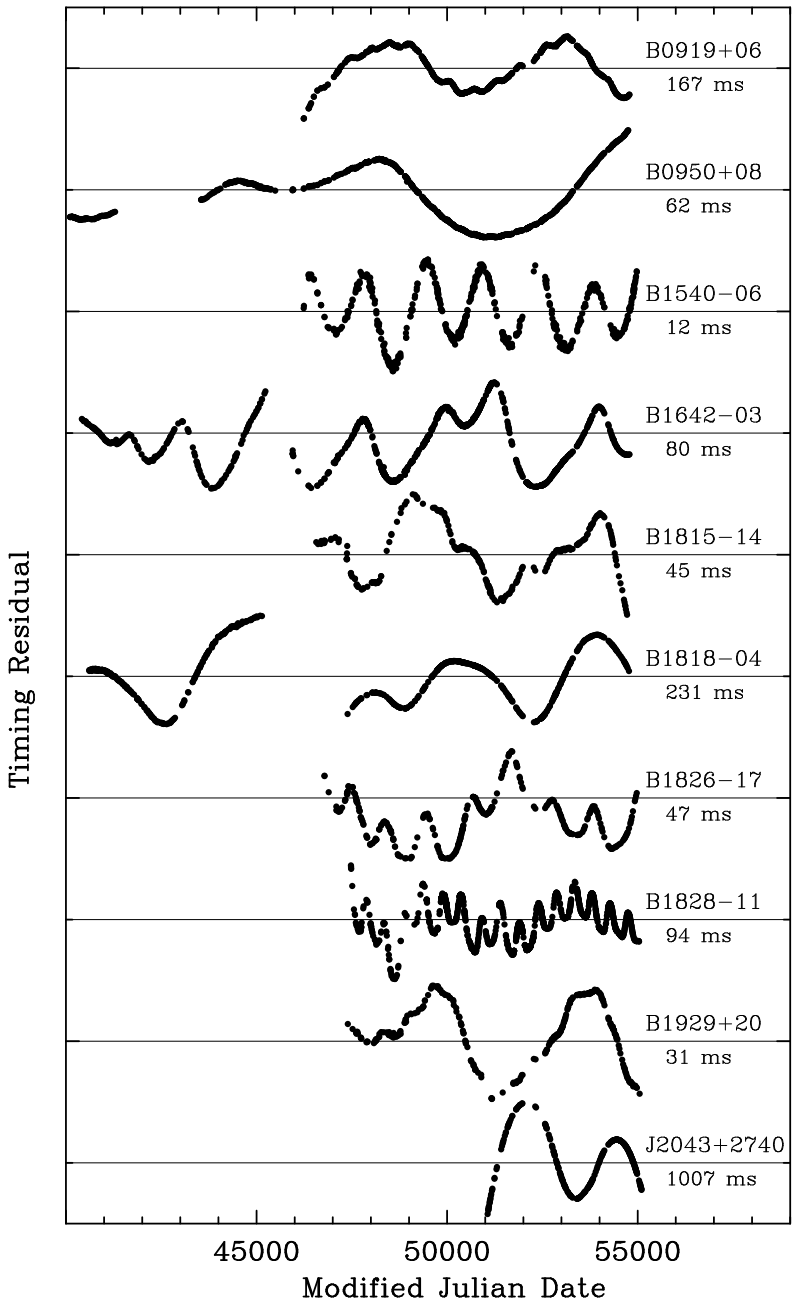
B0919+06
167 ms
B0950+08
62 ms
B1540−06
12 ms
B1642−03
80 ms
B1815−14
45 ms
B1818−04
231 ms
B1826−17
47 ms
B1828−11
94 ms
B1929+20
31 ms
J2043+2740
1007 ms
Timing Residual
45000
50000
55000
Modified Julian Date

Figure 1:

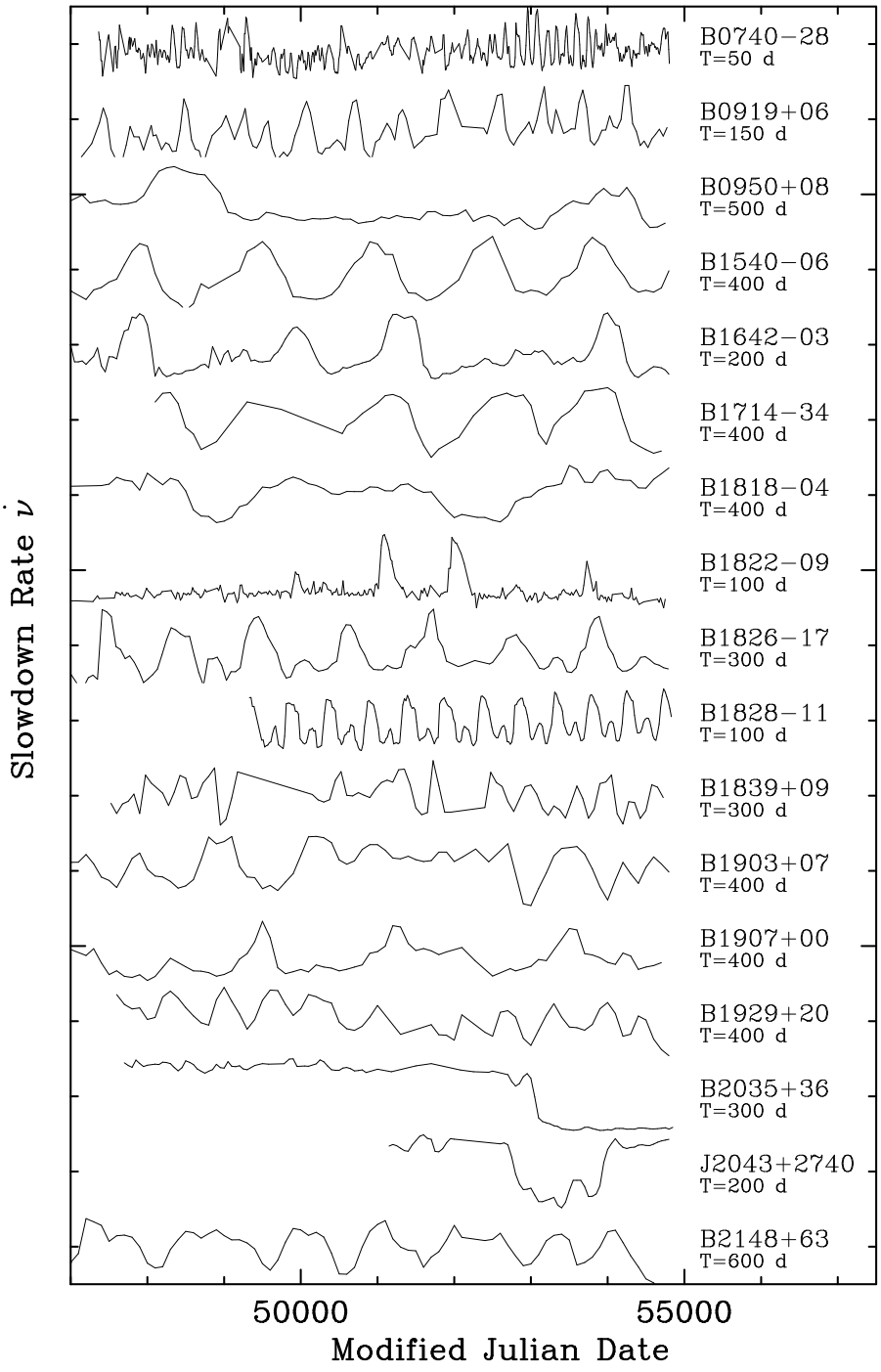
B0740−28
T=50 d
B0919+06
T=150 d
B0950+08
T=500 d
B1540−06
T=400 d
B1642−03
T=200 d
B1714−34
T=400 d
B1818−04
T=400 d
B1822−09
T=100 d
B1826−17
T=300 d
B1828−11
T=100 d
B1839+09
T=300 d
B1903+07
T=400 d
B1907+00
T=400 d
B1929+20
T=400 d
B2035+36
T=300 d
J2043+2740
T=200 d
B2148+63
T=600 d
Slowdown Rate $\dot{\nu}$
50000
55000
Modified Julian Date

Figure 2:

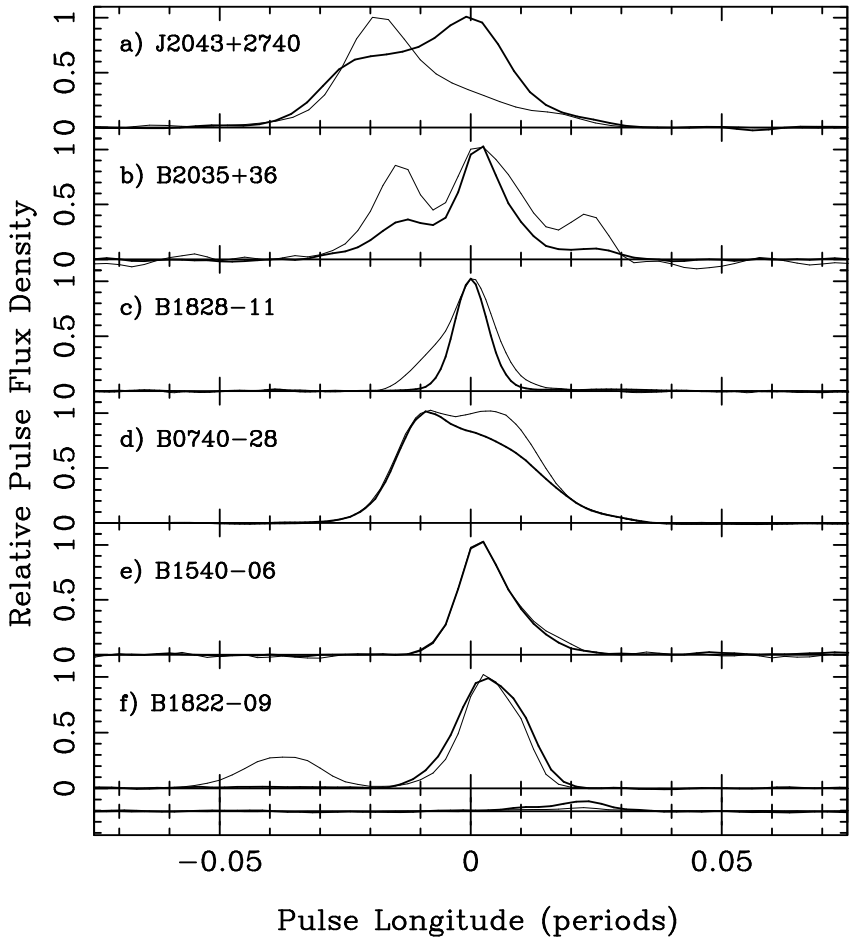
a) J2043+2740
b) B2035+36
c) B1828−11
d) B0740−28
e) B1540−06
f) B1822−09
Relative Pulse Flux Density
0 0.5 1 0 0.5 1 0 0.5 1 0 0.5 1 0 0.5 1 0 0.5 1
−0.05
0
0.05
Pulse Longitude (periods)

Figure 3:

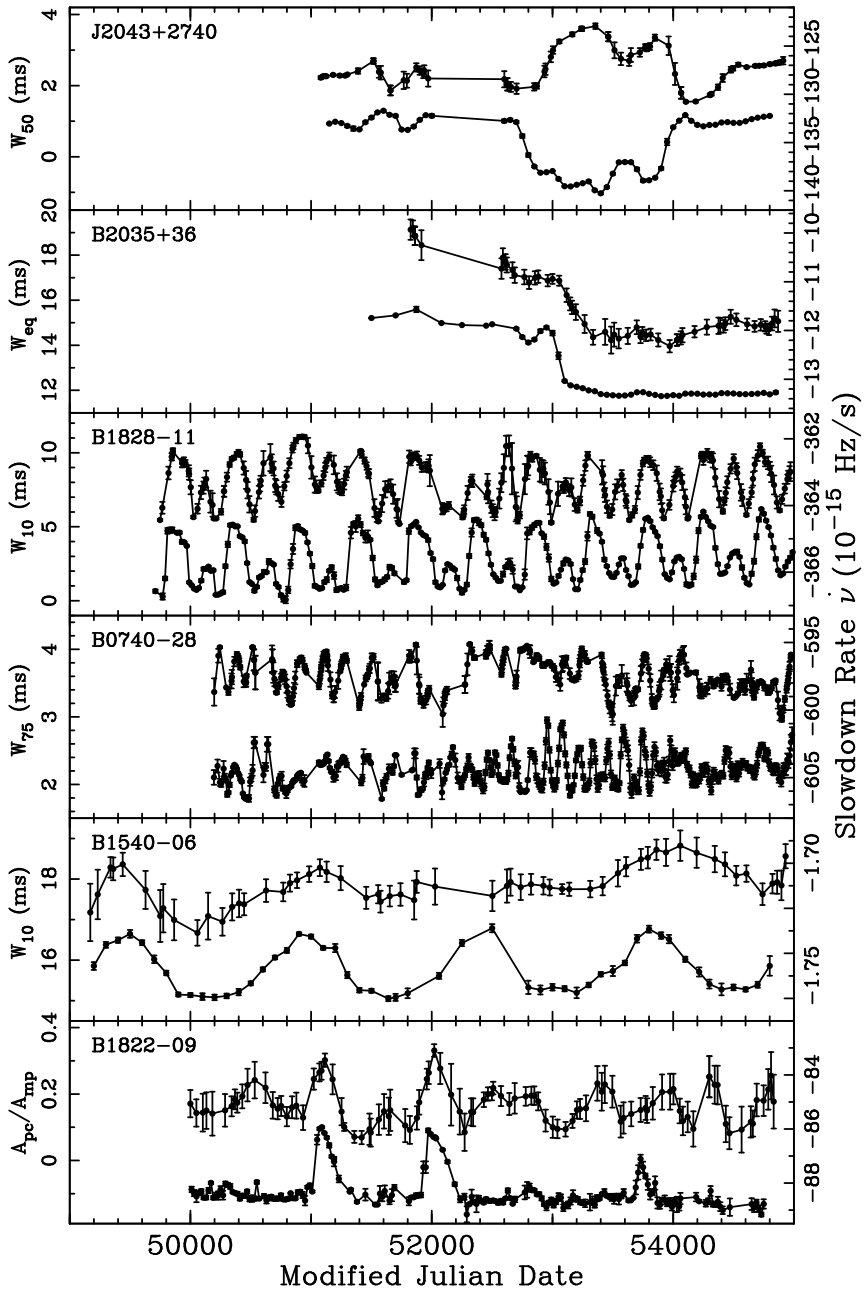
J2043+2740
B2035+36
B1828−11
B0740−28
B1540−06
B1822−09
W50 (ms)
Weq (ms)
W10 (ms)
W75 (ms)
W10 (ms)
Ape/Amp
Slowdown Rate ν̇ (10−15 Hz/s)
Modified Julian Date
50000
52000
54000

Figure 4:

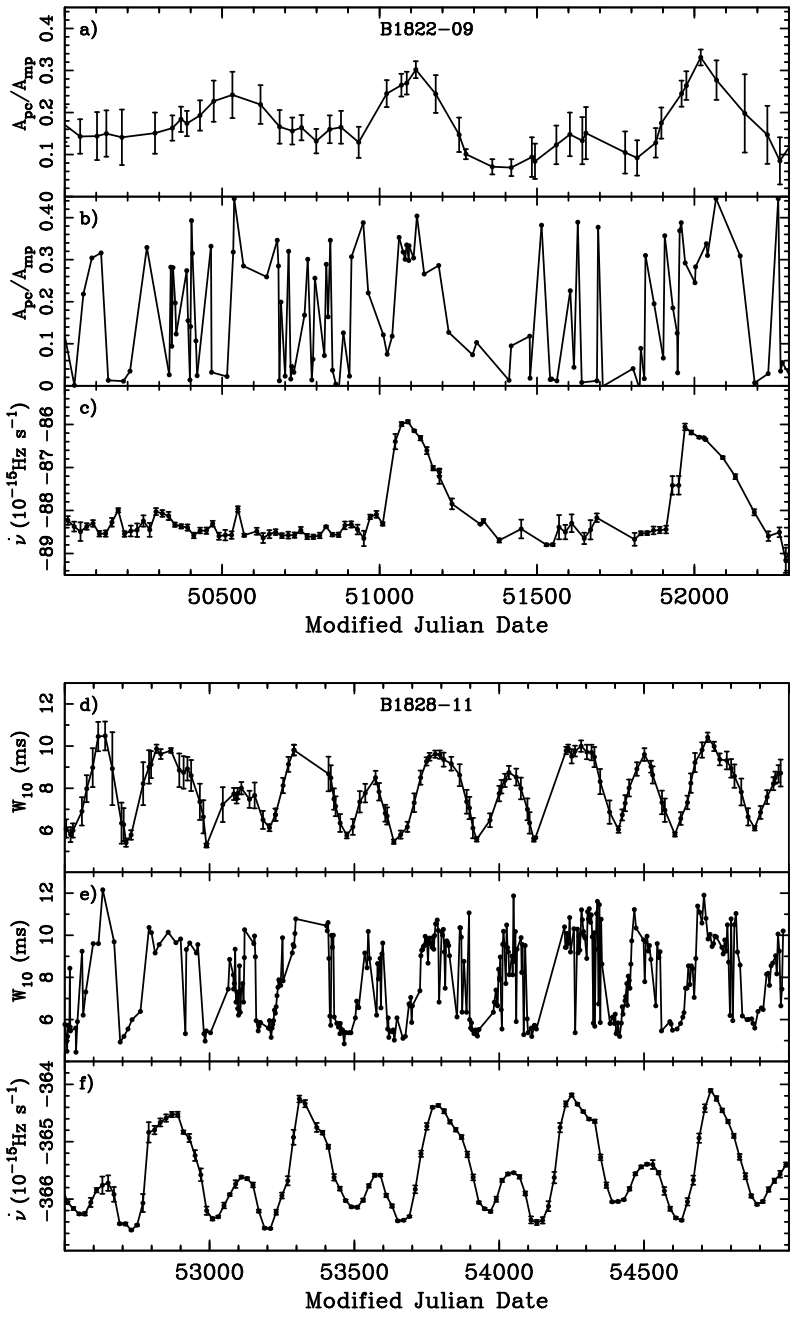
a)
B1822−09
A_{pc}/A_{mp}
b)
A_{pc}/A_{mp}
c)
$\dot{\nu}$ (10^{-15}Hz s^{-1})
Modified Julian Date
d)
B1828−11
W_{10} (ms)
e)
W_{10} (ms)
f)
$\dot{\nu}$ (10^{-15}Hz s^{-1})
Modified Julian Date

Figure 5:

Supporting Online Material

Determining pulse shape parameters

The pairs of pulse profiles in Fig. 3 of the journal paper were inspected and fitted with two or three gaussian components, as required to provide satisfactory descriptions of the profiles. The same components were fitted to each observed profile, and a synthetic profile produced, from which the value of the chosen shape parameter used in Fig. 4 of the journal paper was determined. W_{10}, W_{50} and W_{75} are the widths measured at 10%, 50% and 75% of the pulse peak. $W_{\rm eq}$ is the equivalent width, being the area under the pulse divided by the peak amplitude, and $A_{\rm pc}/A_{\rm mp}$ is the ratio of the peak amplitudes of the precursor and main pulse components. Note that this procedure has the virtue of applying a quasi-optimum filter to the data in order to minimise the effects of high-frequency noise on the values of the parameters.

Determining times-of-arrival

We note that the times-of-arrival used to derive the timing residuals of Fig. 1 in the journal paper were usually obtained by matching the observed pulse profiles with templates derived from average profiles obtained over large sections of the data. Hence, for the objects in Fig. 3 of the journal paper, the templates have intermediate shapes, and are usually not perfectly matched to the observed profile, giving rise to possible systematic offsets in the timing residuals. The maximum magnitudes of the offsets have been estimated by comparing the times-of-arrival obtained by fitting the two profiles in Fig. 3 with the corresponding template. For the six objects, the differences in the offsets were respectively 0.70, 0.05, 0.25, 0.17, 0.04, and 0.14 ms. Since these are much smaller than the variations seen in Fig. 1 of the journal paper, we conclude that the profile switching and use of a single template has little impact upon the structures seen in the timing residuals. In practice, for PSR B1828−11 the procedure described in (*Ref 1 of SoM*) was used and therefore the TOAs are not prone to such systematic errors.

Observational limitations

Within the relatively small number of the pulsars in our sample which have high signal-to-noise ratio profiles, pulse-shape variations are observed which are correlated with spin-down rate. The results show that multiple pulse-profile and associated spin-down states that switch on timescales of weeks to years is a common phenomenon seen in many pulsars. We believe that it is possible that all pulsars which display timing noise may show the same correlated pulse-shape behaviour, although it is so far unobserved in most pulsars, because of a combination of modest profile changes, poor signal-to-noise ratio and often relatively-short available data spans. The profile changes may be small, for instance, if changes in the pulsar emission beam happen to be small in that part of the beam which crosses the line-of-sight to the Earth.

Simulations of timing residuals (Fig. 6)

We have calculated some simulations of a two-state spin-down model for pulsar timing noise in which only two parameters determine the form of the simulations, namely the ratio R of time spent in high and low spin-down states, and the rms fractional dither D in the switching period. In detail, simulated values of $\dot{\nu}$ were determined for a regular time sampling. $\dot{\nu}$ switched between two modes $\dot{\nu}_1$ and $\dot{\nu}_2$, spending a time t_1 in the first mode and t_2 in the second mode (typically t_1 and t_2 are a few hundred days). The ratio of t_1 and t_2 equals R. For simulations involving dithering the timescales, t_1 and t_2 are slightly modified by adding a Gaussian random deviate with an rms of Dt_1 and Dt_2 respectively. The resulting $\dot{\nu}$ values are numerically integrated twice to produce pulse phase, followed by appropriate sampling and a quadratic polynomial removed to form the resulting simulated timing residuals. Note how dither in the switching period can give rise to low-frequency structure in the residuals (Fig. 6c).

References and Notes

1. I. H. Stairs, A. G. Lyne, S. Shemar, *Nature* **406**, 484 (2000).

2. G. Hobbs, A. G. Lyne, M. Kramer, *MNRAS* **402**, 1027 (2010).

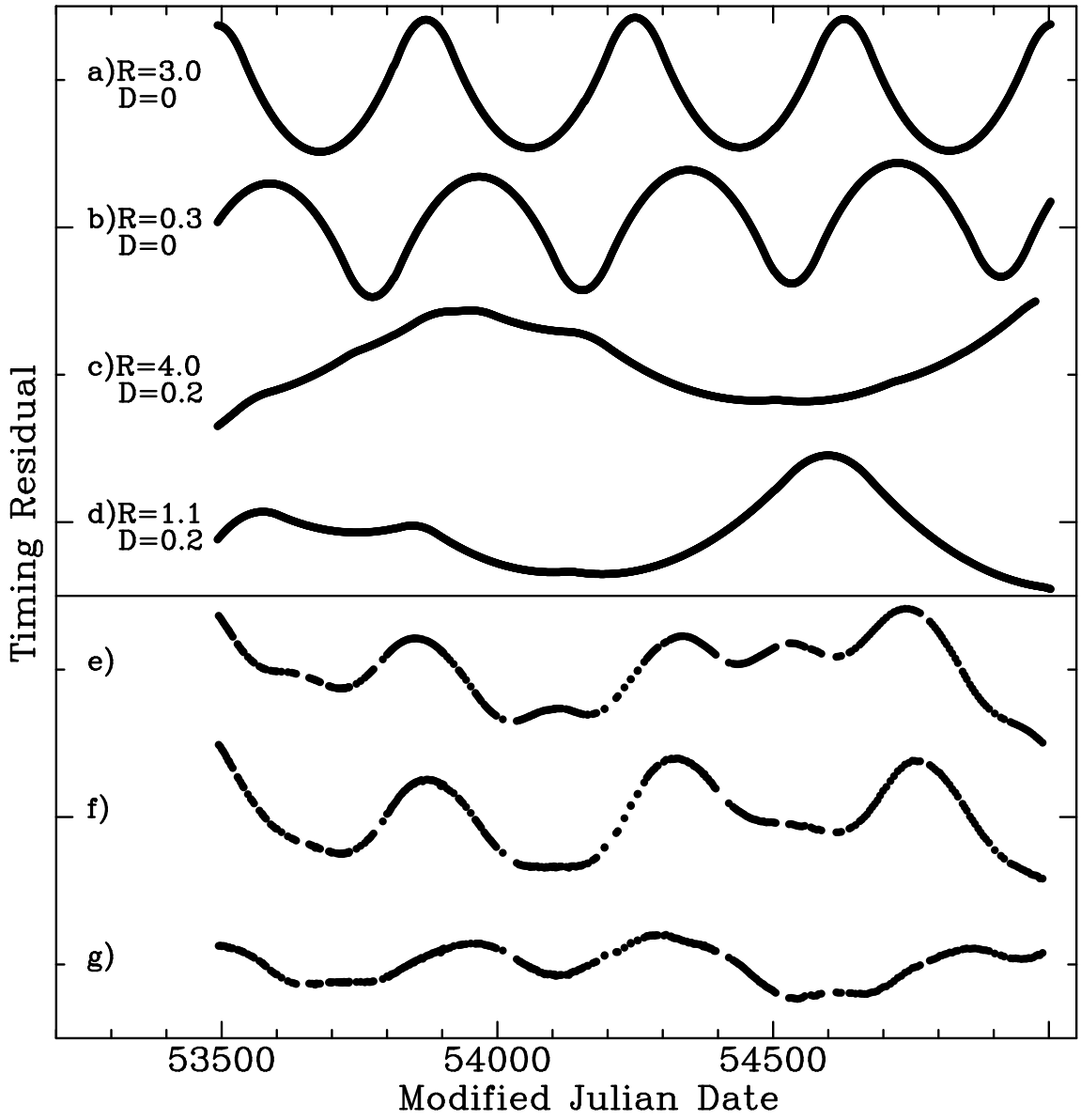

Figure 6: Simulations of timing residuals. a)-d) Simulations of a two-state spin-down model for pulsar timing noise in which only two parameters determine the form of the simulations, namely the ratio R of time spent in high and low spin-down states, and the rms fractional dither D in the switching period (See supporting text). Note how dither in the switching period can give rise to low-frequency structure in the residuals. e) simulated timing residuals for PSR B1828−11 in which the spin-down state is determined purely from the observed pulse shape parameter f) observed timing residuals for PSR B1828−11 from a simple spin-down model, which shows most of the features predicted by e), and g) the difference between the observed and simulated timing residuals. In spite of the severe undersampling of the shape parameter due to telescope availability ($< 1\%$ of the time), this demonstrates how it might be possible to "correct" the times-of-arrival for spin-state variations indicated by the pulse shape.

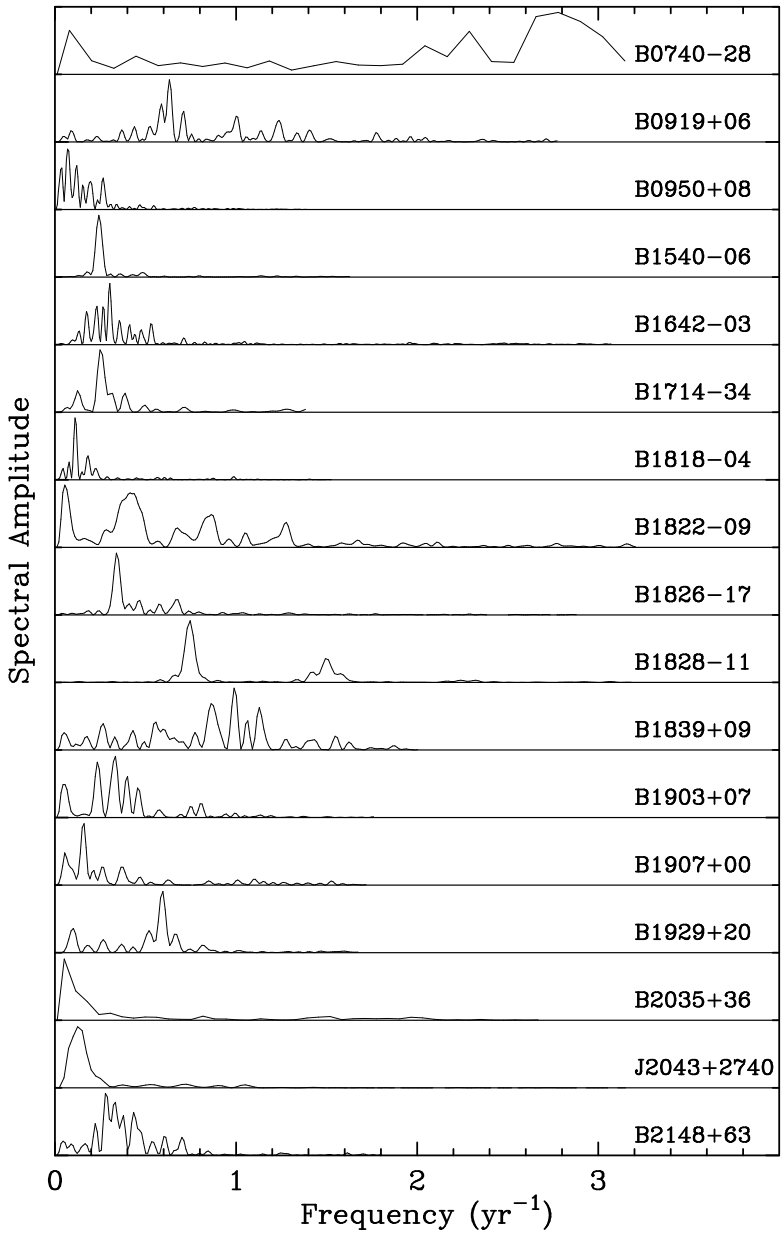

Figure 7: Lomb-Scargle spectra of the spin-down rates $\dot{\nu}$ presented in Fig. 2 of the journal paper for 17 pulsars. The peaks of all the spectra have been normalised to the same amplitude.

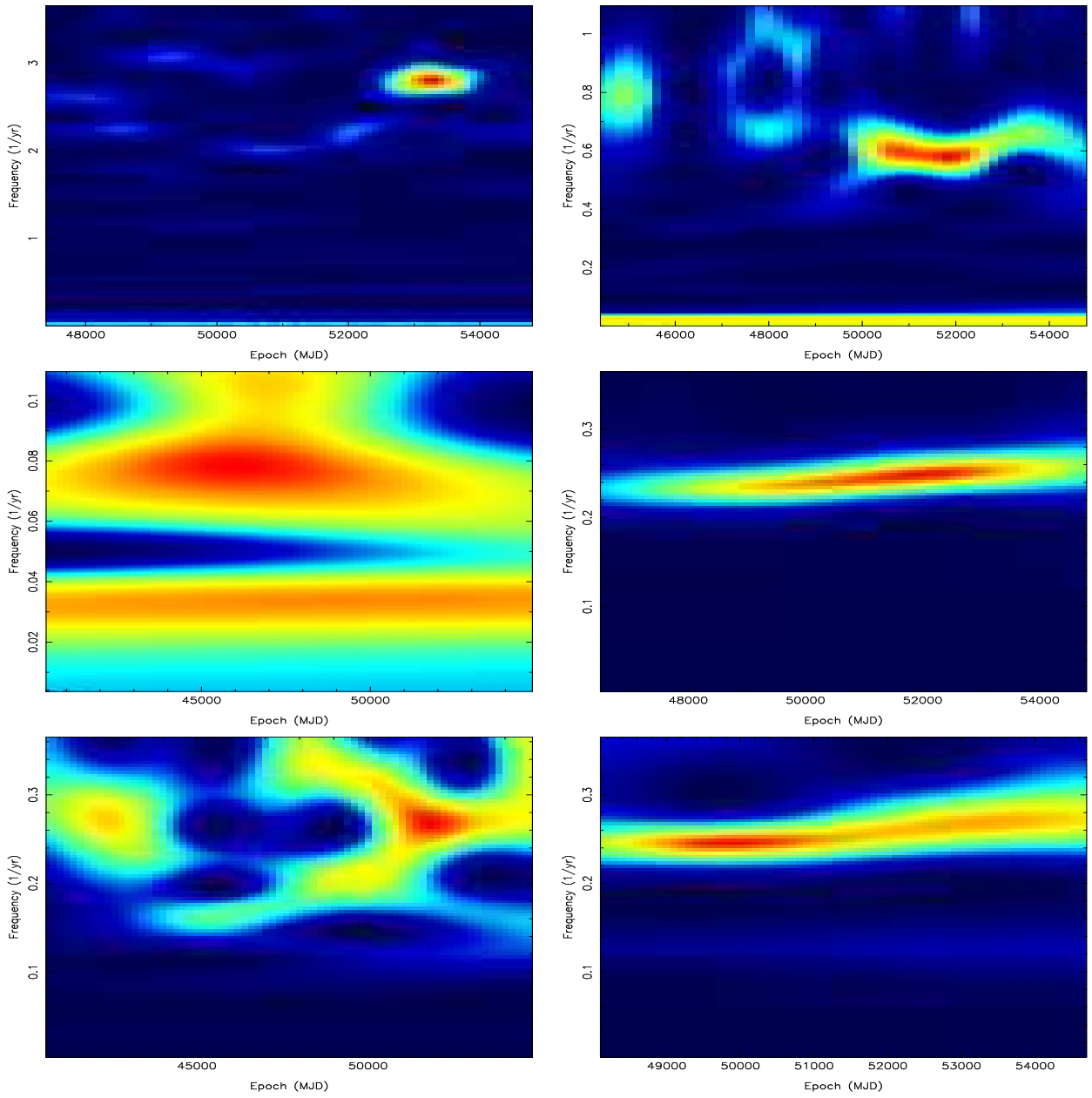

Figure 8: a) Wavelet spectra for pulsars B0740−28 and B0919+06 (top row), B0950+08 and B1540−06 (middle row) and B1642−03 and B1714−34 (bottom row). The frequency ranges shown cover the periodicities suggested in Fig. 7. The wavelet Z-statistic is computed as a function of both time and frequency. The wavelet "window" can be specified by a "decay constant", c, that defines the number of cycles of a given frequency f expected within the window. Values between 0.001 and 0.01 were chosen in an attempt to obtain the best compromise between frequency and time resolution, given the data in Fig. 2. The results agree well with the periodicities derived from the Lomb-Scargle analysis but demonstrate that for some sources the effective frequencies are varying or not always present.

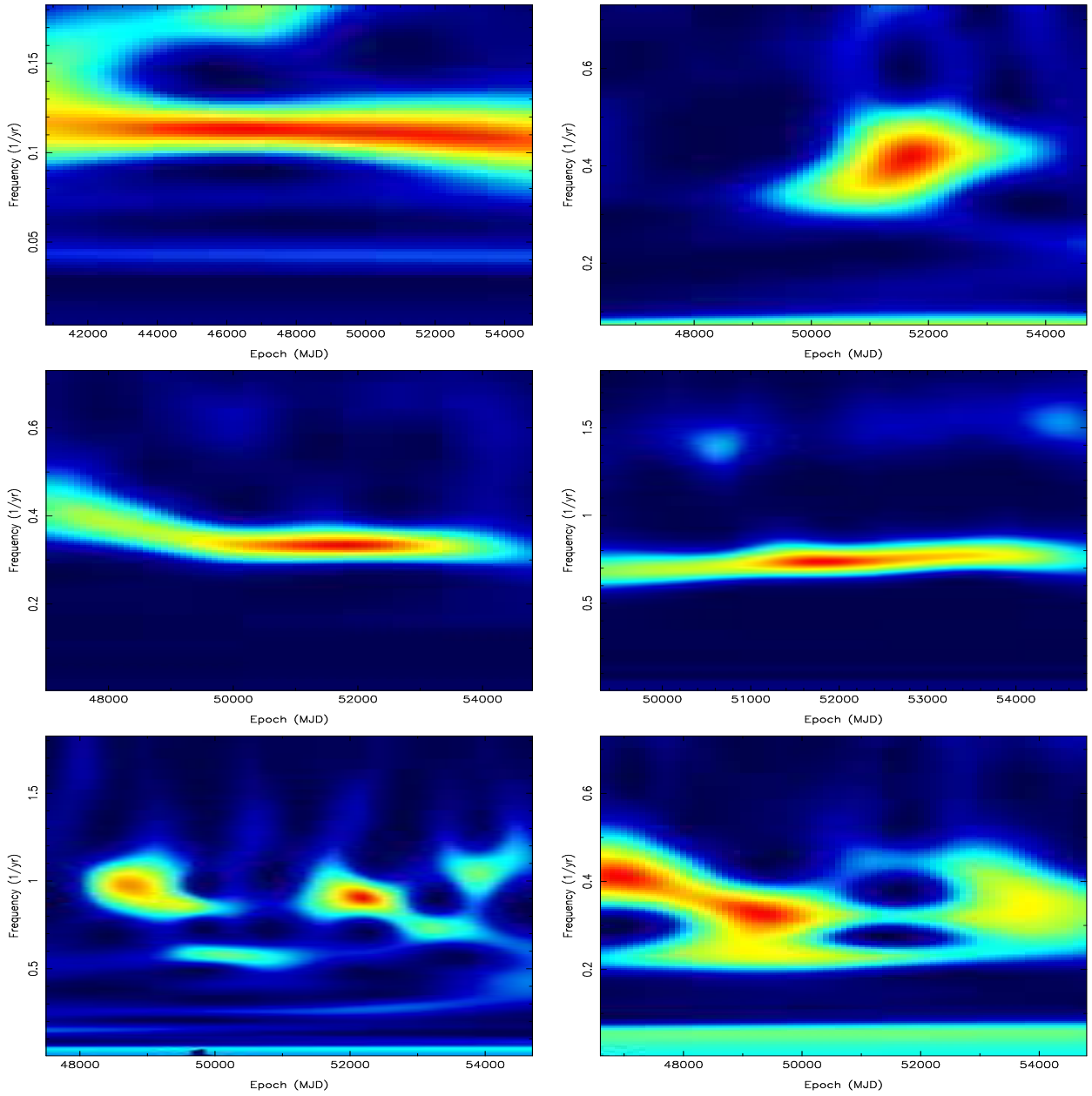

Figure 8: b) Wavelet spectra for pulsars B1818−04 and B1822−09 (top row), B1826−17 and B1828−11 (middle row) and B1839+09 and B1903+07 (bottom row).

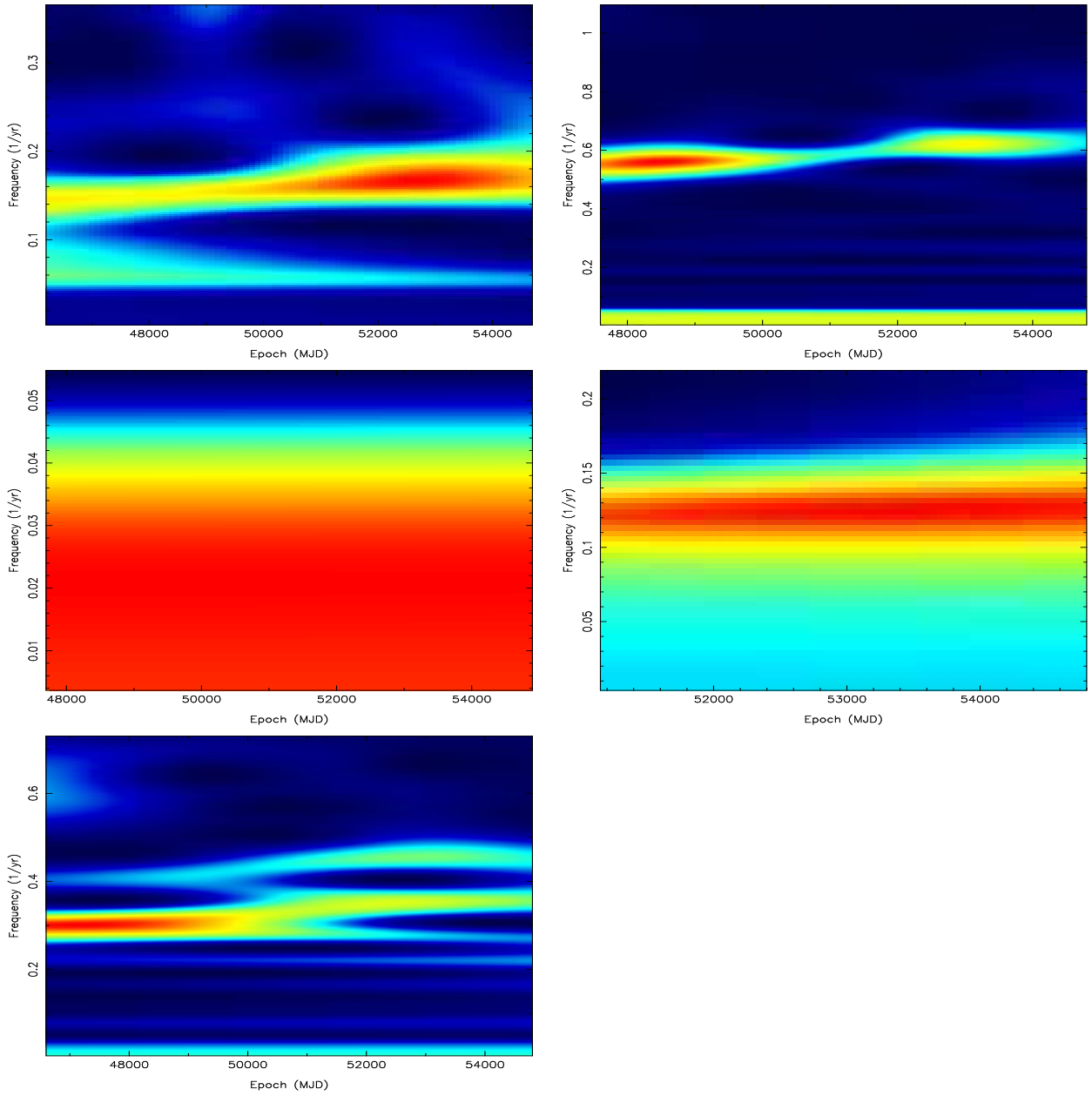

Figure 8: c) Wavelet spectra for pulsars B1907+00 and B1929+20 (top row), B2035+36 and J2043+2740 (middle row) and B2148+63 (bottom row).

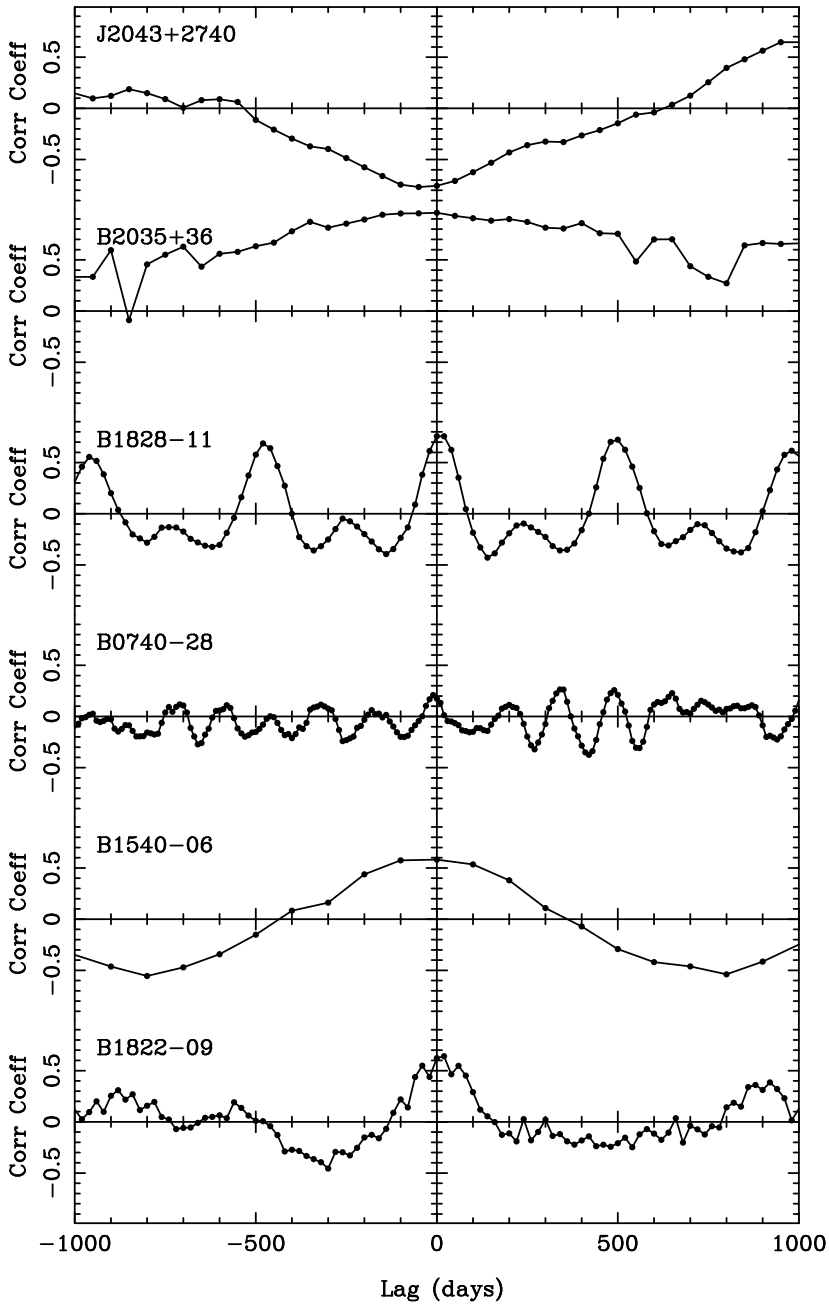

Figure 9: Cross-correlation functions between the average values of pulse shape parameters and the spin-down rates $\dot{\nu}$ shown in Fig. 4 of the journal paper for six pulsars. Note that in all cases, the magnitude of correlation coefficient always peaks close to zero lag.

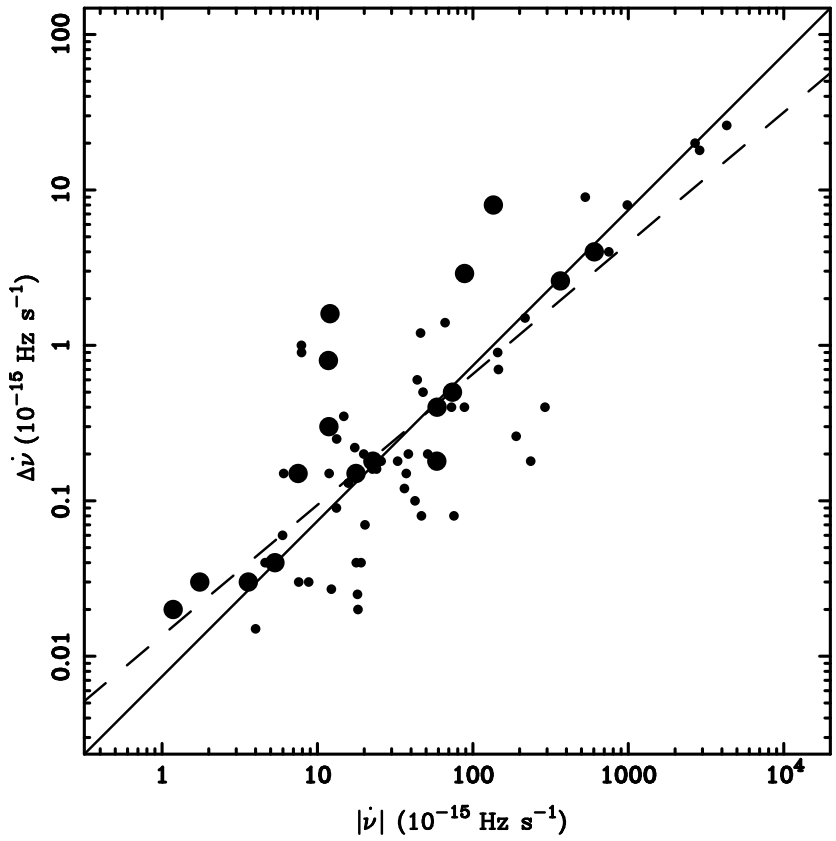

Figure 10: The dependence of the magnitude of the switching in $\dot{\nu}$ upon the magnitude of the average spin-down rate $|\dot{\nu}|$ for the 17 pulsars in Table 1 excepting PSR B1931+24 (large symbols) and another 51 pulsars which were studied in (*Ref 2 of SoM*) (small symbols). There is an excellent correlation between the logarithm of the variables with a correlation coefficient of 0.80. The solid line has a slope of unity and the dashed line is the best-fitting straight line, which has a slope of 0.84 ± 0.08.